WIND INTERACTION MODELS FOR GAMMA-RAY BURST AFTERGLOWS: THE CASE FOR TWO TYPES OF PROGENITORS

Roger A. Chevalier and Zhi-Yun Li
Department of Astronomy, University of Virginia, P.O. Box 3818
Charlottesville, VA 22903; rac5x@virginia.edu, zl4h@virginia.edu

ABSTRACT

Beginning with the γ-ray bursts GRB 970228 and GRB 970508, a standard model for the interpretation of GRB afterglows emerged involving synchrotron emission from a constant energy blast wave expanding into a constant density, "interstellar" medium. However, a massive star origin for GRBs implies a stellar wind environment, probably a Wolf-Rayet star, and we have previously suggested wind interaction models for the afterglows of GRBs 980326, 980519, and 980425/SN 1998bw. Here, we extend the theory of afterglows in winds, considering strong cooling phases, the transition to nonrelativistic motion, jets, and prompt, reverse shock emission. The optical prompt emission in the wind case is expected to be weaker than in interstellar interaction for similar parameters. We examine the afterglows of other well-observed GRBs in the context of wind interaction models, and find that GRBs 970228 and 970508 are likely wind interactors. The revision in the nonthermal afterglow emission from GRB 970228 caused by the recognition of late supernova emission favors wind interaction. The radio evolution of GRB 970508 provides especially strong evidence for wind interaction. For GRB 970508, the observations suggest a density that is compatible with that expected in a Wolf-Rayet star wind. Finally, observations of the afterglow evolution of GRBs 990123 and 990510 and the prompt optical emission from GRB 990123 favor interstellar interaction models, which would suggest compact star merger progenitors for these objects.

Subject headings: gamma-rays: bursts — stars: mass loss — stars: supernovae: general

1. INTRODUCTION

The fireball model for GRBs (gamma-ray bursts) led to predictions of the afterglow emission that might be expected when the energetic shock wave encountered the surrounding medium (Katz 1994; Mészáros, & Rees 1997). The subsequent optical and X-ray observations of the afterglow from GRB 970228 appeared to confirm the predictions of the simplest afterglow model (Wijers, Rees, & Mészáros 1997). This model involved synchrotron emission from electrons accelerated to a power law energy spectrum in a relativistic blast wave expanding into a constant

density, presumably interstellar medium (ISM). In particular, the expected relation between the flux spectral index and the power law rate of flux decay was in approximate accord with the observations. This model has become the "standard model" for the interpretation of GRB afterglow observations. It was used to make predictions of bright optical emission in the early phases when a reverse shock front is present (Sari & Piran 1999b). The observation of a bright flash from GRB 990123 (Akerlof et al. 1999) gave basic confirmation of this aspect of the model (Sari & Piran 1999a; Mészáros & Rees 1999). The expectation of jets for the initial energy deposition led to predictions of the effects on the light curve as the jet slowed (Rhoads 1997, 1999; Sari, Piran, & Halpern 1999). The observations of the afterglow of GRB 990510 confirmed the basic features expected for jet deceleration (Harrison et al. 1999).

These successes of the standard model give confidence that it is essentially correct. However, there has been increasing evidence that at least some GRBs have massive star progenitors, as initially suggested by Woosley (1993) on theoretical grounds. Paczyński (1998) noted that the available evidence on the location of GRBs in their host galaxies indicated a link to star formation. A more direct link to massive stars is provided by the presence of a supernova, the light from the exploded star matter. GRB 980425 was probably associated with the relatively nearby Type Ic supernova SN 1998bw (Galama et al. 1998d; Kulkarni et al. 1998), and evidence for supernova type emission has now been found in GRB 980326 (Bloom et al. 1999b) and GRB 970228 (Reichart 1999; Galama et al. 1999b).

The importance of a massive star origin for the afterglow evolution is that the GRB blast wave should be expanding into the stellar wind of the progenitor star. Dai & Lu (1998), Mészáros, Rees, & Wijers (1998) and Panaitescu, Mészáros, & Rees (1998) described some features of afterglow evolution in a $\rho \propto r^{-2}$ stellar wind. Chevalier & Li (1999, hereafter CL) made specific estimates for expansion into the wind of a Wolf-Rayet star. Li & Chevalier (1999) and CL identified GRB 980425/SN 1998bw, GRB 980326, and GRB 980519 as likely circumstellar wind interactors based on their afterglow evolution. In the cases of GRB 980425 and 980326, this association is supported by the presence of supernova emission. The case for a supernova in GRB 980519 is equivocal (CL). CL identified GRB 990123 as a likely interstellar interactor based on its afterglow evolution. GRBs of this type are not expected to be accompanied by supernovae.

CL placed the afterglows of GRB 980519 and GRB 980326 in the wind category partly based on their relatively rapid rates of decline of optical emission. An alternative explanation for the decline is that the emission is from a jet (Sari, Piran, & Halpern 1999; Halpern et al. 1999). However, in the case of GRB 980519, CL were able to use radio observations made during the first 3 days (Frail et al. 1998b) to further constrain the model. The available data do appear to be consistent with the expectations for wind interaction.

In view of the increasing evidence for massive star progenitors of GRBs, our aim here is to further develop the theory of wind interaction and to examine the data on afterglows in the context of wind and interstellar interaction models. In § 2, we extend the theory of afterglows in

winds to consider strong cooling, nonrelativistic evolution, and jets. Our discussion is guided by previous discussions of the constant density interaction case, and we contrast the two situations. The differences are expected to be especially significant for prompt emission because of the large difference in the ambient density at early times. We treat prompt, reverse shock emission for the wind case in § 3. In § 4, we examine the data on the best observed afterglows in the context of the wind and constant density models. We find that wind models can explain a number of observations previously regarded as puzzling, pointing to wind interaction models for these cases. Although wind models are indicated for the majority of well observed afterglows, there are a number that are better described by constant density interaction. We discuss some implications of this result in § 5. Our conclusions are listed in § 6.

2. AFTERGLOW LIGHT CURVES IN WINDS

2.1. Blast Wave Hydrodynamics

The basic model for GRB afterglow hydrodynamics involves a relativistic blast wave expanding into the surrounding medium (e.g., Mészáros & Rees 1997). During the very early evolution, the GRB ejecta play a role and we treat the hydrodynamics of that phase in § 3. The later blast wave, which is dominated by the energy deposited in the external medium, can be described by a self-similar solution (Blandford & McKee 1976). The solution for expansion in a constant density medium has been widely used in GRB studies and here we discuss some of the basic results for a medium with density $\rho = Ar^{-s}$. The main problem is to determine the blast wave characteristics seen by an external observer.

For an ultrarelativistic, adiabatic blast wave, Blandford & McKee (1976, their eq. [69]) find that

$$E = \frac{8\pi A \Gamma^2 R^{3-s} c^2}{17 - 4s}, \tag{1}$$

where E is the total energy, Γ is the Lorentz factor of the shock front, and R is the shock wave radius. The ultrarelativistic shock condition yields the Lorentz factor of the gas, $\gamma = \Gamma/\sqrt{2}$. Because E is constant, we have the standard result $\gamma \propto R^{-(3-s)/2}$. For an observer viewing the blast wave along the line of sight to the center (not at a cosmological distance), consideration of emission from the blast wave at two times in the blast wave frame yields the time in the observer's frame (e.g., Sari 1997; Dai & Lu 1998):

$$t = \frac{R_L}{4(4-s)\gamma_L^2 c}, \tag{2}$$

where the subscript L refers to the line of sight. For $s = 0$, we have $t = R_L/(16\gamma_L^2 c)$, as in Sari (1997). For the wind case considered here ($s = 2$), we have $t = R_L/(8\gamma_L^2 c)$ (Dai & Lu 1998). The blast wave is undecelerated for $s = 3$ and we obtain $t = R_L/(4\gamma_L^2 c)$; this can also be expressed as

$t = R_L/(2\Gamma_L^2 c)$, which is the standard result for a point moving toward the observer at constant velocity. Substitution into eq. (1) then yields

$$R_L = \left[\frac{(4-s)(17-4s)Et}{4\pi Ac}\right]^{1/(4-s)}. \tag{3}$$

We then have $R_L = (17Et/\pi\rho_o c)^{1/4}$, where ρ_o is the ambient density, for $s = 0$ and $R_L = (9Et/2\pi Ac)^{1/4}$ for $s = 2$.

The problem with these expressions is that they apply only to the line of sight. In observing a burst, the emission can be dominated by emission away from the center because the burst is observed at an earlier time when it may have been brighter. The appearance depends on the evolution of the burst, which itself depends on the observing frequency. Sari (1998) has considered these issues for a blast wave in a constant density medium and found that the typical radius and Lorentz factor are $0.80R_L$ and $1.4\gamma_L$ at low frequency and $0.67R_L$ and $1.8\gamma_L$ at high frequency. In our case ($s = 2$), there is less deceleration so we expect smaller deviations from the line of sight values. We estimate typical values $R = 0.8R_L$ and $\gamma = 1.1\gamma_L$ where the relation between R and γ follows the $\gamma \propto R^{-1/2}$ relation expected for a blast wave in an $s = 2$ medium. We thus have for a distant observer

$$R = 2.9 \times 10^{17} \left(\frac{1+z}{2}\right)^{-1/2} E_{52}^{1/2} A_\star^{-1/2} t_{\rm day}^{1/2} \text{ cm} \tag{4}$$

and

$$\gamma = 4.2 \left(\frac{1+z}{2}\right)^{1/4} E_{52}^{1/4} A_\star^{-1/4} t_{\rm day}^{-1/4}, \tag{5}$$

where E_{52} is the blast wave energy in units of 10^{52} ergs, $t_{\rm day}$ is the observer's time in units of days, $A = \dot{M}_{\rm w}/4\pi V_{\rm w} = 5 \times 10^{11} A_\star$ g cm^{-1}, $\dot{M}_{\rm w}$ is the mass loss rate, and $V_{\rm w}$ is the wind velocity. The reference value of A corresponds to $\dot{M}_{\rm w} = 1 \times 10^{-5}\ M_\odot$ yr^{-1} and $V_{\rm w} = 1000$ km s^{-1}. In addition, the cosmological redshift z enters because of time dilation.

2.2. Afterglow Properties with Slow Cooling

Our treatment of afterglow light curves in winds follows the discussions of afterglows in a constant density interstellar medium (Rees & Mészáros 1997; Waxman 1997; Sari, Piran, & Narayan 1998). We presume that electrons are accelerated in the blast wave shock wave to a power energy distribution, $N(\gamma) \propto \gamma^{-p}$ for $\gamma > \gamma_m$ where γ_m is the minimum Lorentz factor at the shock front. The synchrotron spectrum of the afterglow can be divided into 4 power law sections that are separated at 3 characteristic frequencies: the synchrotron self-absorption frequency ν_A, the characteristic frequency ν_m emitted by electrons with Lorentz factor γ_m, and the frequency at which synchrotron losses become important ν_c (Sari et al. 1998). If the frequencies are ordered $\nu_A < \nu_m < \nu_c$, the four sections of the spectrum can be described by $F_\nu \propto \nu^\beta$ with $\beta = 2, 1/3, -(p-1)/2, -p/2$ going from low to high frequency. The observations of GRB 970508

on day 12 can be represented by this spectrum (Galama et al. 1998b) and we initially assume this ordering of the characteristic frequencies in this section. The slow cooling condition can be expressed as $\nu_m < \nu_c$ (Sari et al. 1998). The peak flux, $F_{\nu,\max}$, occurs at ν_m for this case.

In any power law segment of the spectrum, the flux evolution is expected to follow a power law $F_\nu \propto \nu^\beta t^\alpha$. For a constant density medium ($s = 0$), the standard result is $\alpha = -3(p-1)/4 = 3\beta/2$ for $\nu_m < \nu < \nu_c$ and $\alpha = -(3p-2)/4 = (3\beta+1)/2$ for $\nu_c < \nu$. In a wind ($s = 2$), we have $\alpha = -(3p-1)/4 = (3\beta-1)/2$ for $\nu_m < \nu < \nu_c$ and the same evolution as the $s = 0$ case for $\nu_c < \nu$. A signature of wind interaction afterglows in the adiabatic, high frequency phase of evolution is a relatively rapid rate of decline. The plausible assumption that most of the electron energy is near γ_m requires $p > 2$ and $\alpha < -1.25$. Many optical afterglows are observed to initially have $\alpha \gtrsim -1.3$ and so are unlikely to be in the adiabatic, wind category. However, if the optical emission is in the cooling regime, $\alpha = -(3p-2)/4$ as in the $s = 0$ case and the requirement $p > 2$ implies $\alpha < -1.0$. More candidate afterglows are potentially in this category, but there is the additional requirement of a moderately steep observed spectral index: $\beta = -p/2$ so that $p > 2$ implies $\beta < -1.0$.

The observed values of $F_{\nu,\max}$, ν_m, ν_A, and ν_c have been used to find the blast wave energy E, ambient density n, electron energy fraction ϵ_e, and magnetic energy fraction ϵ_B in the context of $s = 0$ models (Wijers & Galama 1999; Granot et al. 1999). In wind models, the constant density is replaced by the wind density $\rho = Ar^{-2}$, where $A = \dot{M}_{\rm w}/4\pi V_{\rm w} = 5 \times 10^{11} A_\star$ g cm^{-1}, as discussed below eq. (5). In CL, expressions were derived for the characteristic frequencies and $F_{\nu,\max}$ in terms of the model parameters. We repeat the expressions for completeness:

$$F_{\nu,\max} = 20 \left(\frac{\sqrt{1+z}-1}{\sqrt{2}-1}\right)^{-2} \left(\frac{1+z}{2}\right)^{1/2} \left(\frac{\epsilon_B}{0.1}\right)^{1/2} E_{52}^{1/2} A_\star t_{\rm day}^{-1/2} \text{ mJy}, \tag{6}$$

$$\nu_A \approx 1 \times 10^{11} \left(\frac{1+z}{2}\right)^{-2/5} \left(\frac{\epsilon_e}{0.1}\right)^{-1} \left(\frac{\epsilon_B}{0.1}\right)^{1/5} E_{52}^{-2/5} A_\star^{6/5} t_{\rm day}^{-3/5} \text{ Hz}, \tag{7}$$

$$\nu_m = 5 \times 10^{12} \left(\frac{1+z}{2}\right)^{1/2} \left(\frac{\epsilon_e}{0.1}\right)^{2} \left(\frac{\epsilon_B}{0.1}\right)^{1/2} E_{52}^{1/2} t_{\rm day}^{-3/2} \text{ Hz}, \tag{8}$$

$$\nu_c \approx 2 \times 10^{12} \left(\frac{1+z}{2}\right)^{-3/2} \left(\frac{\epsilon_B}{0.1}\right)^{-3/2} E_{52}^{1/2} A_\star^{-2} t_{\rm day}^{1/2} \text{ Hz}, \tag{9}$$

where our expressions assume a flat universe with $H_o = 65$ km s^{-1} Mpc^{-1}. We also assume that the composition of the wind gas is H depleted and that the electron spectral index is $p \approx 2.5$; the variation due to different values of p is less than other uncertainties. We now invert these expressions in order to solve for the model parameters. The observations are taken to all refer to the same day, t. Then

$$E \approx 3 \times 10^{52} y^3 x^{-1/2} \left(\frac{t}{\rm day}\right)^{-1/2} \left(\frac{F_{\nu,\max}}{\rm mJy}\right)^{3/2} \left(\frac{\nu_A}{10^9 \text{ Hz}}\right)^{-5/6} \left(\frac{\nu_m}{10^{12} \text{ Hz}}\right)^{-5/12} \left(\frac{\nu_c}{10^{14} \text{ Hz}}\right)^{1/4} \text{ergs}, \tag{10}$$

$$A_\star \approx 9 \times 10^{-4} x \left(\frac{t}{\rm day}\right)^{2} \left(\frac{\nu_A}{10^9 \text{ Hz}}\right)^{5/3} \left(\frac{\nu_m}{10^{12} \text{ Hz}}\right)^{5/6} \left(\frac{\nu_c}{10^{14} \text{ Hz}}\right)^{1/2}, \tag{11}$$

$$\epsilon_e \approx 0.006\ y^{-1}x^{1/2}\left(\frac{t}{\rm day}\right)^{3/2}\left(\frac{F_{\nu,\rm max}}{\rm mJy}\right)^{-1/2}\left(\frac{\nu_A}{10^9\ \rm Hz}\right)^{5/6}\left(\frac{\nu_m}{10^{12}\ \rm Hz}\right)^{11/12}\left(\frac{\nu_c}{10^{14}\ \rm Hz}\right)^{1/4}, \quad (12)$$

$$\epsilon_B \approx 1\times 10^2 yx^{-5/2}\left(\frac{t}{\rm day}\right)^{-5/2}\left(\frac{F_{\nu,\rm max}}{\rm mJy}\right)^{1/2}\left(\frac{\nu_A}{10^9\ \rm Hz}\right)^{-5/2}\left(\frac{\nu_m}{10^{12}\ \rm Hz}\right)^{-5/4}\left(\frac{\nu_c}{10^{14}\ \rm Hz}\right)^{-5/4}, \quad (13)$$

where

$$x = \frac{1+z}{2} \qquad \text{and} \qquad y = \frac{\sqrt{2x}-1}{\sqrt{2}-1}.$$

The afterglow light curve depends on how the break frequencies and the peak flux, $F_{\nu,\rm max}$, evolve with time and here we consider the light curve without cooling. As in Sari et al. (1998) for the ISM case, we can define critical times at which the break frequencies pass through a fixed frequency ν. The time that ν_m crosses the observed frequency is

$$t_m = 60\left(\frac{1+z}{2}\right)^{1/3}\left(\frac{\epsilon_e}{0.1}\right)^{4/3}\left(\frac{\epsilon_B}{0.1}\right)^{1/3}E_{52}^{1/3}\nu_{10}^{-2/3}\ \text{days}, \quad (14)$$

where ν_{10} is ν in units of 10^{10} Hz. The time that ν_A crosses the observed frequency is

$$t_A = 50\left(\frac{1+z}{2}\right)^{-2/3}\left(\frac{\epsilon_e}{0.1}\right)^{-5/3}\left(\frac{\epsilon_B}{0.1}\right)^{1/3}E_{52}^{-2/3}A_\star^2\nu_{10}^{-5/3}\ \text{days}. \quad (15)$$

Provided $t_A < t_m$, the light is as follows: $F_\nu \propto R^2 \propto t$ for $t < t_A$, $F_\nu \propto F_{\nu,\rm max}\nu_m^{-1/3} \propto t^0$ for $t_A < t < t_m$, and $F_\nu \propto F_{\nu,\rm max}\nu_m^{(p-1)/2} \propto t^{-(3p-1)/4}$ for $t_m < t$. The condition that $t_A = t_m$ leads to a critical time and frequency:

$$t_{Am} = 80\left(\frac{1+z}{2}\right)\left(\frac{\epsilon_e}{0.1}\right)^{10/3}\left(\frac{\epsilon_B}{0.1}\right)^{1/3}E_{52}A_\star^{-4/3}\ \text{days}, \quad (16)$$

and

$$\nu_{Am} = 7\times 10^9\left(\frac{1+z}{2}\right)^{-1}\left(\frac{\epsilon_e}{0.1}\right)^{-3}E_{52}^{-1}A_\star^2 \quad \text{Hz}. \quad (17)$$

For $\nu > \nu_{Am}$, the light curve is as described above. For $\nu < \nu_{Am}$, the flat part of the light curve is no longer present and the evolution goes directly from $F_\nu \propto t$ to $F_\nu \propto t^{-(3p-1)/4}$. In this regime, the peak flux and its frequency evolve as $F_{\nu,\rm max} \propto t^{-2p/(p+3)}$ and $\nu_{\rm max} \propto t^{-3(p+1)/2(p+3)}$; the expressions for ν_A and ν_m (eqs. [7] and [8]) no longer apply. It can be seen from the estimated value of ν_{Am} that these considerations are relevant to radio observations of afterglows.

2.3. Fast Cooling Case

The description of the evolution given in CL and in §2.2 assumes that $\nu_m < \nu_c$. Although synchrotron cooling is important for the high energy electrons, it is not important for the electrons emitting near ν_m which have most of the energy. Before some time, t_o, when $\nu_m = \nu_c$, cooling of these lower energy electrons is rapid compared to the age and this phase can be referred to as

having fast cooling (Sari et al. 1998). If ϵ_e is close to 1 and the electron energy couples to the ion and magnetic energy, the blast wave steadily loses energy and the hydrodynamic evolution is termed radiative. If these conditions are not met, the hydrodynamic evolution is approximately adiabatic even for $t < t_o$. We consider this second case to be the most likely and concentrate on it. For $\nu_m > \nu_c$, the expressions for $F_{\nu,\rm max}$, ν_m, and ν_c (eqs. [6], [8], and [9]) remain unchanged; the maximum flux now occurs at ν_c instead of ν_m. The spectrum can be described by $F_\nu \propto \nu^\beta$ with $\beta = 1/3, -1/2, -p/2$ going from low to high frequency and the breaks at ν_c and ν_m, respectively (Sari et al. 1998). However, eq. (7) for ν_A is no longer applicable. We ignore synchrotron self-absorption in our initial discussion of the fast cooling case.

Eqs. (8) and (9) imply that

$$t_o = 2 \left(\frac{1+z}{2}\right) \left(\frac{\epsilon_e}{0.1}\right) \left(\frac{\epsilon_B}{0.1}\right) A_\star \text{ days}. \tag{18}$$

For standard parameters, the transition to slow cooling occurs at a later time for the wind case compared to the ISM case because of the higher densities that the shock front encounters at early times.

The afterglow light curve again depends on how the break frequencies and the peak flux, $F_{\nu,\rm max}$, evolve with time. The cooling time for the wind case is

$$t_c = 2 \times 10^{-5} \left(\frac{1+z}{2}\right)^3 \left(\frac{\epsilon_B}{0.1}\right)^3 E_{52}^{-1} A_\star^4 \nu_{10}^2 \text{ days}. \tag{19}$$

Cooling of the radiating electrons is important before t_c and not after, which is the opposite of the ISM case. The time that ν_m crosses ν is given by eq. (14). There are two possible orderings for the three times: $t_m < t_o < t_c$ and $t_c < t_o < t_m$. These cases are divided by a critical frequency, $\nu_o = \nu_c(t_o) = \nu_m(t_o)$:

$$\nu_o = 3 \times 10^{12} \left(\frac{1+z}{2}\right)^{-1} \left(\frac{\epsilon_e}{0.1}\right)^{1/2} \left(\frac{\epsilon_B}{0.1}\right)^{-1} E_{52}^{1/2} A_\star^{-3/2} \text{ Hz}. \tag{20}$$

When $\nu > \nu_o$, the ordering $t_m < t_o < t_c$ applies and the evolution can be called the high-frequency light curve (cf. Sari et al. 1998 for the ISM case). The evolution is described by $F_\nu \propto t^{-1/4}\nu^{-1/2}$ $(t < t_m)$, $t^{-(3p-2)/4}\nu^{-p/2}$ $(t_m < t < t_o)$, $t^{-(3p-2)/4}\nu^{-p/2}$ $(t_o < t < t_c)$, and $t^{-(3p-1)/4}\nu^{-(p-1)/2}$ $(t_c < t)$. When $\nu < \nu_o$, $t_c < t_o < t_m$ applies and we have the low-frequency light curve: $F_\nu \propto t^{-1/4}\nu^{-1/2}$ $(t < t_c)$, $t^{-2/3}\nu^{1/3}$ $(t_c < t < t_o)$, $t^0\nu^{1/3}$ $(t_o < t < t_m)$, and $t^{-(3p-1)/4}\nu^{-(p-1)/2}$ $(t_m < t)$. These light curves are distinct from the ISM case, especially because of the early importance of cooling.

Self-absorption is important throughout the cooling regime ($t < t_o$) if $t_A > t_o$. From eqs. (16) (which assumes the low-frequency light curve) and (18), the frequency at which $t_A = t_o$ is given by

$$\nu_{Ao} = 8 \times 10^{10} \left(\frac{1+z}{2}\right)^{-1} \left(\frac{\epsilon_e}{0.1}\right)^{-8/5} \left(\frac{\epsilon_B}{0.1}\right)^{-2/5} E_{52}^{-2/5} A_\star^{3/5} \text{ Hz}. \tag{21}$$

With typical parameters, $\nu_{Ao} < \nu_o$ so that the use of eq. (16) is justified. At radio wavelengths, the synchrotron emission is self-absorbed during the fast cooling period and we have $F_\nu \propto t$. At optical and X-ray wavelengths, self-absorption is important only during the early phases of the fast cooling period.

Finally, we briefly discuss the expected evolution for a radiative blast wave (cf. Blandford & McKee 1976; Vietri 1997; Sari et al. 1998). In this case for a $\rho \propto r^{-2}$ ambient medium, the shocked gas has $\gamma \propto R^{-1}$ so that $R \propto t^{1/3}$. We have $\nu_c \propto t^{1/3}$ and $F_{\nu,\max} \propto t^{-2/3}$ so that $F_\nu = F_{\nu,\max}(\nu/\nu_c)^{-1/2} \propto \nu^{-1/2}t^{-1/2}$ for $\nu > \nu_c$ and $F_\nu = F_{\nu,\max}(\nu/\nu_c)^{1/3} \propto \nu^{1/3}t^{-7/9}$ for $\nu < \nu_c$.

2.4. Transition to Nonrelativistic Evolution

The transition to nonrelativistic evolution has been discussed for the ISM, constant density case by Wijers et al. (1997) and Waxman, Kulkarni, & Frail (1998). For an ambient density $\rho = Ar^{-2}$, a straightforward estimate of the transition radius and time is when the shock has swept up a mass equivalent to the rest mass of the explosion:

$$r_{\rm NR} = \frac{E}{4\pi Ac^2} = 1.8 \times 10^{18} \frac{E_{52}}{A_\star} \text{ cm} \tag{22}$$

and

$$t_{\rm NR} = \frac{r_{\rm NR}}{c} = 1.9(1+z)\frac{E_{52}}{A_\star} \text{ yr.} \tag{23}$$

From eq. (5), the relativistic blast wave shock Lorentz factor at this time is $\Gamma = 1.15$.

The nonrelativistic blast wave in a $\rho = Ar^{-2}$ medium is particularly simple for adiabatic index $\gamma_a = 5/3$ (cf. Sedov 1959). The shock radius is given by

$$r_s = \left(\frac{3E}{2\pi A}\right)^{1/3} t^{2/3} \tag{24}$$

and the postshock profiles are $\rho = \rho_s(r/r_s)$, $v = v_{gs}(r/r_s)$, and $p = p_s(r/r_s)^3$, where the subscript s refers to the value at the shock front and v_{gs} is the gas velocity at the shock front. The blast wave expansion can be described by $r_s = \xi_o(E/A)^{1/3}t^{2/3}$, where $\xi_o = 0.78$ if $\gamma_a = 5/3$ (nonrelativistic fluid) and $\xi_o = 0.64$ if $\gamma_a = 4/3$ (relativistic fluid). The $\gamma_a = 5/3$ evolution yields $\dot{r}_s/c = 1.2$ at the time $t_{\rm NR}$. The relativistic and nonrelativistic expansion approximately cross at $t_{\rm NR}$, showing that this is a reasonable estimate of the transition time. Eq. (23) shows that the transition to nonrelativistic evolution in a wind is late for typical parameters; the expected value of $t_{\rm NR}$ is longer than the typical duration of observations of GRB afterglows.

In considering the evolution during the nonrelativistic regime, the treatment is similar to that in the relativistic regime provided $\gamma_m \gtrsim 1$. We have $R \propto t^{2/3}$, shock velocity $v_{sh} \propto t^{-1/3}$, $\rho_1 v_{sh}^2 \propto t^{-2}$, $B \propto t^{-1}$, and $\gamma_m \propto v_{sh}^2 \propto t^{-2/3}$, so that $\nu_m \propto \gamma_m^2 B \propto t^{-7/3}$ and $F_{\nu_m} \propto NB \propto Rt^{-1} \propto t^{-1/3}$, where ρ_1 is the preshock density and N is the total number of radiating particles. Then,

$F_\nu \propto F_{\nu_m}\nu_m^{-1/3} \propto t^{4/9}$ ($\nu < \nu_m$) and $F_\nu \propto F_{\nu_m}\nu_m^{(p-1)/2} \propto t^{(5-7p)/6}$ ($\nu > \nu_m$). For example, $p = 3$ yields $F_\nu \propto t^{-8/3}$ in the nonrelativistic case for $\nu > \nu_m$, but $F_\nu \propto t^{-2}$ in the relativistic case. As in interstellar interaction, the light curve steepens after the transition to nonrelativistic flow.

2.5. Jets

In most models for GRBs, the burst energy is initially deposited in a relativistic jet. As long as the jet is highly relativistic, the observed features should be reproduced by spherical models, but as the shocked jet slows there are effects on the observed light curve (as first discussed by Rhoads 1997). If θ_o is the angular width of the jet, the edge of the jet becomes visible when $\gamma \approx \theta_o^{-1}$ (Panaitescu & Mészáros 1999). The other important effect is that the slowed jet is able to expand laterally. Rhoads (1997, 1999) estimates that this will occur when $\gamma \approx \theta_o^{-1}/\sqrt{3}$, but Sari, Piran, & Halpern (1999) argue that the transition occurs when $\gamma \approx \theta_o^{-1}$. The issue is the speed of sideways expansion and 2-dimensional numerical simulations may be needed to provide reliable results. The important point is that during the spreading phase, there is exponential slowing down of the forward shock front (Rhoads 1997). Rhoads (1999) has discussed this phenomenon in detail for interstellar interaction, but suggests that it also occurs for expansion in a wind.

Because jet effects are expected when $\gamma \approx \theta_o^{-1}$, eq. (5) can be used to find the time

$$t_{\rm jet} = 1 \left(\frac{1+z}{2}\right) \left(\frac{\theta_o}{0.2}\right)^4 E_{52} A_\star^{-1} \text{ day} \tag{25}$$

when jet effects become important. A steepening of the afterglow light curve is expected at this time. Once lateral spreading of the jet becomes important, the exponential slowing implies that R becomes essentially constant with time and this defines the hydrodynamic evolution (Sari et al. 1999). If the exponential slowing does occur for wind interaction, both ISM and wind interactors should show the same emission properties during the spreading phase. We expect $F_\nu \propto t^0\nu^2$ ($\nu < \nu_A$), $t^{-1/3}\nu^{1/3}$ ($\nu_A < \nu < \nu_m$), $t^{-p}\nu^{-(p-1)/2}$ ($\nu_m < \nu < \nu_c$), and $t^{-p}\nu^{-p/2}$ ($\nu_c < \nu$) (Sari et al. 1999).

3. PROMPT, REVERSE SHOCK EMISSION

An initially relativistically hot fireball associated with a GRB cools as it expands, forming a cold shell of material coasting at an ultrarelativistic speed when most of the internal energy is converted into the bulk kinetic energy. When the coasting shell runs into an ambient medium, the bulk kinetic energy is gradually released back into the internal energy, which gives rise to prompt emission. Prompt emission has been discussed by Sari & Piran (1999a,b) and Mészáros & Rees (1999) in the context of GRB 990123, both assuming a constant ambient density suitable for the interstellar medium. Here, we extend their discussion of prompt emission to the case of interaction with a surrounding stellar wind.

The structure of the coasting shell is largely unknown, and is determined by the way that mass and energy are injected from the central engine. It is likely to be inhomogeneous, since bursts of gamma rays are thought to come from one part of the shell running into another. We shall, however, ignore such inhomogeneities and adopt uniform distributions for both the shell density and Lorentz factor (denoted by $\gamma_{\rm sh}$) for simplicity.

As is well known, the shell interacts with the ambient medium via two shocks: a forward shock and a reverse shock. The forward shock runs forward into the ambient medium, whereas the reverse shock sweeps up the shell material. The shocked ambient and shell materials are in pressure balance and are separated by a contact continuity. Since the thickness of the shocked region is expected to be much smaller than its radius, the whole interaction region can be treated as planar, as done by Katz (1994) and Sari & Piran (1995). We will follow these authors in determining the shock properties in a planar geometry, assuming in addition that only a small fraction of the internal energy of the shocked materials is radiated away by electrons.

There are four regions of distinct properties: the unshocked ambient medium (denoted by "1"), the shocked ambient medium (denoted by "2"), the shocked shell material (denoted by "3") and the unshocked coasting shell (denoted by "4"). We assume that the shocked materials in regions 2 and 3 are uniform and move together, and thus share a common bulk Lorentz factor. From relativistic shock jump conditions, we find that the Lorentz factor is

$$\gamma_{12} = \frac{\xi^{1/4}\gamma_{\rm sh}^{1/2}}{\sqrt{2}}, \tag{26}$$

(measured relative to the nearly static ambient medium, region 1) where $\xi \equiv \rho_4/\rho_1$ is the ratio of proper mass densities in the unshocked shell (region 4) and the ambient medium (region 1). The proper mass density in the ambient medium is given by

$$\rho_1 = \frac{\dot{M}_{\rm w}}{4\pi R^2 V_{\rm w}}, \tag{27}$$

where $\dot{M}_{\rm w}$ and $V_{\rm w}$ are the mass loss rate and the velocity of the ambient wind, and R the spherical radius. The proper density of the unshocked shell is given by

$$\rho_4 = \frac{M_{\rm sh}}{4\pi R^2 \gamma_{\rm sh}\Delta}, \tag{28}$$

where $M_{\rm sh}$ and Δ are the proper mass and the width (measured in the frame at rest with respect to the origin and the ambient medium) of the initial shell. The proper mass is related to the total initial kinetic energy E_0 of the coasting shell through

$$M_{\rm sh} = \frac{E_0}{\gamma_{\rm sh} c^2}, \tag{29}$$

where c is the speed of light. From equations (27)-(29), we have

$$\xi = \frac{E_0 V_{\rm w}}{\dot{M}_{\rm w}\gamma_{\rm sh}^2 c^2 \Delta}, \tag{30}$$

which is independent of radius. Therefore, the shocked materials move at a constant speed according to equation (26). This fact simplifies our discussion of their emission properties.

The initial shell width Δ is unknown a priori. It is related to the time in the observer's frame, $t_{\rm cr}$, for the reverse shock to cross the entire shell through

$$t_{\rm cr} = \frac{1+z}{2}\frac{\Delta}{c}, \tag{31}$$

where z is the cosmological redshift of the GRB. The timescale $t_{\rm cr}$ characterizes the duration of prompt emission. We assume that the duration is comparable to that of the GRB itself, which is typically 10's of seconds for the sources with observed afterglows. That is, the shell needs to have a width of tens of light seconds or more. We shall therefore scale Δ by 10 light seconds, and denote the scaled width by Δ_{10}. Scaling other quantities with their typical values, we have

$$\xi = 65\frac{E_{52}}{A_\star \Delta_{10}\gamma_{300}^2}, \tag{32}$$

where γ_{300} is $\gamma_{\rm sh}$ divided by 300. In deriving equation (31), we have assumed that $\xi \ll \gamma_{\rm sh}^2$, which is true for typical parameters. Substituting equation (32) into equation (26), we finally have

$$\gamma_{12} = 35\frac{E_{52}^{1/4}}{A_\star^{1/4}\Delta_{10}^{1/4}}, \tag{33}$$

which is much greater than unity unless Δ_{10}, the most uncertain parameter in the above expression, is unreasonably large.

The shocked ambient medium and the shocked shell material have not only the same bulk Lorentz factor, but also the same internal energy because of pressure balance across the contact discontinuity. Relativistic shock jump conditions yield

$$e_3 = e_2 = 2\gamma_{\rm sh}\rho_1 c^2 \xi^{1/2}, \tag{34}$$

where the mass density of the ambient wind is given by equation (27), which can be rewritten into

$$\rho_1 = \frac{\dot{M}_{\rm w}}{4\pi V_{\rm w} R^2} = \frac{\dot{M}_{\rm w}}{4\pi V_{\rm w} c^2 T^2}, \tag{35}$$

with the time T measured in the frame at rest with respect to the origin. As usual, we assume a (small) fraction ϵ_e of the internal energy of the shocked matter goes into radiating electrons with a power-law energy distribution. Adopting a constant power-law index of p, the minimum electron Lorentz factors in the two shocked regions are

$$\gamma_{m2} = \left(\frac{p-2}{p-1}\right)\left(\frac{2}{1+X}\right)\left(\frac{m_p}{m_e}\right)\frac{\epsilon_{e2}\gamma_{\rm sh}^{1/2}\xi^{1/4}}{\sqrt{2}}, \tag{36}$$

and

$$\gamma_{m3} = \left(\frac{p-2}{p-1}\right)\left(\frac{2}{1+X}\right)\left(\frac{m_p}{m_e}\right)\frac{\epsilon_{e3}\gamma_{\rm sh}^{1/2}}{\sqrt{2}\xi^{1/4}}, \tag{37}$$

where m_p and m_e are the mass of protons and electrons, respectively, and X is the fractional abundance of hydrogen, which is close to zero for Wolf-Rayet winds. In addition, we assume that a constant fraction ϵ_B of the internal energy goes into the magnetic field in both the shocked ambient medium and the shocked shell material, which yields a total field strength of

$$B_{\rm tot} = (8\pi\epsilon_B e_2)^{1/2} = \left(\frac{4\epsilon_B \gamma_{\rm sh} \dot{M}_{\rm w} \xi^{1/2}}{V_{\rm w}}\right)^{1/2} \frac{1}{T}, \tag{38}$$

in regions 2 and 3.

To determine the shock emission properties, we adopt the formalism of Wijers & Galama (1999). Let us first consider the reverse shock (region 3). Ignoring the synchrotron self-absorption for the moment, there are two characteristic frequencies that we need to determine: the "typical" frequency ν_{m3} corresponding to the minimum Lorentz factor γ_{m3} and the cooling frequency ν_c. In the observer's frame, we find

$$\nu_{m3} = \frac{2}{3}\left(\frac{2}{1+z}\right)\left(\frac{3\chi_p}{4\pi}\right)\frac{\gamma_{12}\gamma_{m3}^2\ e\ B_{\rm tot}}{m_e c}$$

$$= 4.0\times10^{18}\chi_p\left(\frac{p-2}{p-1}\right)^2\left(\frac{2}{1+X}\right)^2\left(\frac{\epsilon_{e3}}{0.1}\right)^2\left(\frac{\epsilon_B}{0.1}\right)^{1/2}\frac{A_\star\Delta_{10}^{1/2}\gamma_{300}^2}{E_{52}^{1/2}\ t}\ \ {\rm Hz}, \tag{39}$$

where χ_p is a dimensionless constant whose value is close to half for the expected value of p between 2 and 3 (see Fig. 1 of Wijers & Galama 1999), and t is the time in the observer's frame. The observer's time t (in units of seconds) is related to the time T in the frame at rest with respect to the origin through

$$t = \frac{1+z}{2}\frac{T}{\gamma_{12}^2}. \tag{40}$$

The "typical" frequency ν_{m3} shown in equation (39) is to be compared with the cooling frequency ν_c corresponding to the cooling Lorentz factor

$$\gamma_c = \frac{6\pi m_e c}{\sigma_{_T}\gamma_{12}B_{\rm tot}^2 t}, \tag{41}$$

where $\sigma_{_T}$ is the Thomson cross section. In the observer's frame, we find

$$\nu_c = \frac{2}{3}\left(\frac{2}{1+z}\right)\left(\frac{0.286\times3}{4\pi}\right)\frac{\gamma_{12}\gamma_c^2 eB_{\rm tot}}{m_e c} = 5.1\times10^7\left(\frac{2}{1+z}\right)^4\left(\frac{\epsilon_B}{0.1}\right)^{-3/2}\frac{E_{52}^{1/2}t}{A_\star^2\Delta_{10}^{1/2}}\ \ {\rm Hz}. \tag{42}$$

Clearly, the cooling frequency is much lower than the "typical" frequency for reasonable parameters, indicating that all radiating electrons cool quickly down to the cooling Lorentz factor γ_c. In other words, the shocked shell material is in the fast cooling regime of Sari, Piran & Narayan (1998). The emitted flux therefore peaks at ν_c instead of ν_{m3}, with a peak value given approximately by

$$F_{\nu_c,3} = \frac{N_{e,3}(1+z)\gamma_{12}P'_{\nu'_c}}{4\pi d_{_L}^2}, \tag{43}$$

where the number of radiating electrons $N_{e,3}$ in the shocked shell region increases linearly with time as

$$N_{e,3} = \left(\frac{2}{1+z}\right)\left(\frac{1+X}{2}\right)\frac{E_0 t}{\gamma_{\rm sh} m_p c \Delta}. \quad (44)$$

The power radiated per electron per unit frequency in the rest frame of the shocked material, $P'_{\nu'_c}$, is given by the formula

$$P'_{\nu'_c} = \phi_p \frac{\sqrt{3} e^3 B_{\rm tot}}{m_e c^2}, \quad (45)$$

where ϕ_p is another dimensionless constant whose value is close to half (see again Fig. 1 of Wijers & Galama 1999). The luminosity distance $d_{_L}$ is given by

$$d_{_L} = \frac{2c}{H_0}(1+z-\sqrt{1+z}), \quad (46)$$

where H_0 is the Hubble constant, whose value we shall assume to be 65 km s^{-1} Mpc^{-1}. Substituting equations (44)-(46) to equation (43), we arrive at a peak flux at the cooling frequency of

$$F_{\nu_c,3} = 11\left(\frac{1+X}{2}\right)\left[\frac{\phi_p}{(\sqrt{1+z}-1)^2}\right]\left(\frac{\epsilon_B}{0.1}\right)^{1/2}\frac{E_{52}A_\star^{1/2}}{\gamma_{300}\Delta_{10}} \ \ {\rm Jy}, \quad (47)$$

which is independent of time.

With the two characteristic frequencies (ν_{m3} and ν_c) and the peak flux ($F_{\nu_c,3}$) thus determined, we can now obtain the flux at any given frequency. We are particularly interested in the optical prompt emission, say in R-band at $\nu_{_R} = 4.5\times10^{14}$Hz, a frequency well above the cooling frequency ν_c but below the typical frequency ν_{m3} for typical parameters. In this spectral regime, we have (cf. Sari et al. 1998)

$$F_{\nu_{_R},3} = \left(\frac{\nu_{_R}}{\nu_c}\right)^{-1/2} F_{\nu_c,3}$$

$$= 3.8\left(\frac{2}{1+z}\right)^2\left(\frac{1+X}{2}\right)\left[\frac{\phi_p}{(\sqrt{1+z}-1)^2}\right]\left(\frac{\epsilon_B}{0.1}\right)^{-1/4}\frac{E_{52}^{5/4}t^{1/2}}{A_\star^{1/2}\gamma_{300}\Delta_{10}^{5/4}} \ \ {\rm mJy}. \quad (48)$$

Note that in this case the optical flux increases with the square root of the observer's time, and a maximum is reached when the reverse shock crosses the inner edge of the freely coasting shell at the time

$$t_{\rm cr} = 10\frac{1+z}{2}\Delta_{10} \ \ {\rm s}. \quad (49)$$

The corresponding maximum flux is

$$F^{\rm max}_{\nu_{_R},3} = 12\left(\frac{2}{1+z}\right)^{3/2}\left(\frac{1+X}{2}\right)\left[\frac{\phi_p}{(\sqrt{1+z}-1)^2}\right]\left(\frac{\epsilon_B}{0.1}\right)^{-1/4}\frac{E_{52}^{5/4}}{A_\star^{1/2}\gamma_{300}\Delta_{10}^{3/4}} \ \ {\rm mJy}. \quad (50)$$

Interestingly, the peak flux is not sensitive to the magnetic energy fraction ϵ_B, one of the most uncertain parameters. Note that a flux of 12 mJy in the R-band corresponds to a magnitude of 13.5. Therefore, it is difficult to create a $9^{\rm th}$-magnitude optical flash that lasts for several tens of

seconds, as observed in GRB 990123 (Akerlof et al. 1999), in the reverse shock if the explosion occurs in a typical Wolf-Rayet wind, unless the parameters are far from typical, e.g., a much high explosion energy than 10^{52} ergs (see § 4.3 for a discussion).

For completeness, we now discuss briefly the prompt emission from the forward shock. The ambient medium shocked by the forward shock has the same cooling frequency ν_c as the shell material shocked by the reverse shock, but a substantially higher typical frequency of

$$\nu_{m2} = \frac{2}{3}\left(\frac{2}{1+z}\right)\left(\frac{3\chi_p}{4\pi}\right)\frac{\gamma_{12}\gamma_{m2}^2 eB_{\rm tot}}{m_e c}$$

$$= 2.6\times 10^{20}\chi_p\left(\frac{p-2}{p-1}\right)^2\left(\frac{2}{1+X}\right)^2\left(\frac{\epsilon_{e2}}{0.1}\right)^2\left(\frac{\epsilon_B}{0.1}\right)^{1/2}\frac{E_{52}^{1/2}}{\Delta_{10}^{1/2}t}\ \ {\rm Hz}, \tag{51}$$

where equation (36) is used to eliminate γ_{m2}. For typical parameters, we have $\nu_c < \nu_{_R} < \nu_{m2}$, and the flux in the R-band is given by

$$F_{\nu_{_R},2} = \left(\frac{\nu_{_R}}{\nu_c}\right)^{-1/2}\frac{N_{e,2}(1+z)\gamma_{12}P'_{\nu'_c}}{4\pi d_{_L}^2}, \tag{52}$$

where the number of radiating electrons $N_{e,2}$ in the shocked ambient medium swept up by the forward shock increases linearly with time as

$$N_{e,2} = \left(\frac{1+X}{2}\right)\left(\frac{2}{1+z}\right)\frac{\dot{M}_{\rm w}c\gamma_{12}^2 t}{m_p V_{\rm w}}. \tag{53}$$

Compared with the R-band flux for the reverse shock given in equation (48), the flux in the forward shock is down by a factor of

$$\frac{F_{\nu_{_R},2}}{F_{\nu_{_R},3}} = \frac{N_{e,2}}{N_{e,3}} = \frac{1}{2\xi^{1/2}} = \frac{1}{16.1}\frac{A_\star^{1/2}\Delta_{10}^{1/2}\epsilon_{300}}{E_{52}^{1/2}}. \tag{54}$$

Therefore, the optical flash is typically dominated by the reverse shock, as in the previously studied case of constant-density ambient medium.

After the coasting shell is completely shocked, the reverse shock front disappears, and there is no more shell kinetic energy left to drive the forward shock. Instead of maintaining a constant Lorentz factor, the shocked region slows down with time as more ambient medium is swept up. The forward shock front begins to evolve as described in § 2. For the material in the reverse shock region, we still have $\nu_c < \nu_{m3}$ at the time that the reverse shock disappears. The electrons in this region thus rapidly cool and do not contribute to the emission, which is dominated by the forward shock region.

Synchrotron self-absorption may reduce our estimate of the optical prompt emission. A simple way to gauge this effect is to estimate the maximal flux emitted by the shocked shell material as a black body

$$F_{\nu,{\rm bb}} \approx (1+z)^3\pi\left(\frac{R_\perp}{d_{_L}}\right)^2\left(\frac{2\nu^2}{c^2}\right)kT_{\rm eff}, \tag{55}$$

(Sari & Piran 1999b) with the observed size $R_\perp$ given roughly by

$$R_\perp \approx 2\gamma_{12}ct, \tag{56}$$

and the effective temperature by

$$kT_{\rm eff} \approx \gamma_{12}\gamma_c m_e c^2/3, \tag{57}$$

since most of electrons cool quickly to the Lorentz factor γ_c. Substituting equations (56) and (57) into equation (55), we have

$$F_{\nu,\rm bb} \approx 0.15 \left(\frac{\nu}{\nu_{_R}}\right)^2 \left(\frac{\epsilon_B}{0.1}\right)^{-1} \left(\frac{E_{52}}{A_\star^2 \Delta_{10}}\right) \frac{t^3}{(\sqrt{1+z}-1)^2} \ \ \mu{\rm Jy}, \tag{58}$$

which increases rapidly with time as t^3. At the particular time $t_{\rm cr}$ given in equation (49) when the reverse shock crosses the inner edge of the coasting shell, the black body flux is roughly

$$F^{cr}_{\nu,\rm bb} \approx 0.15 \left(\frac{1+z}{2}\right)^3 \frac{1}{(\sqrt{1+z}-1)^2} \left(\frac{\nu}{\nu_{_R}}\right)^2 \left(\frac{\epsilon_B}{0.1}\right)^{-1} \left(\frac{E_{52}\Delta_{10}^2}{A_\star^2}\right) \ \ {\rm mJy}, \tag{59}$$

which is roughly two orders of magnitude below the (maximum) prompt optical flux at the same time, given by equation (50), for typical parameters. Therefore, it appears that synchrotron self absorption will lower our estimate of optical prompt emission from the reverse shock significantly, unless $A_\star$ and/or ϵ_B are unusually small, and/or E_{52} and/or Δ_{10} are exceptionally large. Finally, we note that the prompt emission estimated here may also be lowered by inverse Compton scattering, which cools the radiating electrons in addition to synchrotron emission (cf. Sari & Piran 1999b)

4. OBSERVED SOURCES

4.1. GRB 970228

A recent development is the finding of evidence for a supernova in GRB 970228 (Reichart 1999; Galama et al. 1999b); the late spectrum is especially convincing. At first sight, this appears to be in conflict with the apparently interstellar nature of the afterglow: Fruchter et al. (1999a) found time evolution with $\alpha = -1.10 \pm 0.05$ at optical wavelengths and the overall evolution appears to be compatible with expansion in a constant density medium (Wijers, Rees, & Mészáros 1997). However, if the late observations are attributed to a supernova, the decline of the nonthermal optical afterglow steepens and $\alpha = -1.58 \pm 0.28$ (Reichart 1999) or $\alpha = -1.73^{+0.09}_{-0.12}$ (Galama et al. 1999b). With a plausible amount of extinction, Reichart (1999) finds $\beta = -0.61 \pm 0.32$ at optical wavelengths. The optical-to-X-ray spectral index is better constrained; Galama et al. (1999b) find $\beta_{oX} = -0.780 \pm 0.022$ at early times. Cooling evolution (ν_c below optical wavelengths) is unlikely because $\beta = -0.78$ would imply $p = 1.56$. With $\beta = -0.78$, an adiabatic blast wave in a constant density medium implies $\alpha = -1.17$, but a blast wave in a wind implies $\alpha = -1.67$ (Mészáros et al.

1998; CL) in good agreement with the observed decline. GRB 970228 can thus be plausibly added to the wind interaction category with $p \approx 2.6$.

The evolution of the X-ray afterglow shows $\alpha = -1.33^{+0.11}_{-0.13}$, $\beta = -0.96 \pm 0.19$ up to day 4 at 2–10 keV (Costa et al. 1997) and $\alpha = -1.50^{+0.35}_{-0.23}$ up to day 10 at 0.1–2.4 keV (Frontera et al. 1998). There is some evidence for a flatter rate of decline at X-ray frequencies compared to the optical, which would suggest that ν_c is below the X-ray regime. Eq. (9) shows that the X-ray emission should be in the cooling regime for $t_d \lesssim 1$ for reasonable values of the parameters. The spectrum may be somewhat flatter than $\beta = -0.78$ in the optical, steepening to $\beta < -1$ in the X-ray regime.

GRB 970228 was observed at radio wavelengths, but was not detected at limits between 10 μJy and 1 mJy over the first year (Frail et al. 1998a). In an interstellar interaction model, the peak flux, $F_{\nu,\rm max}$, should remain constant and move to lower frequency with time. Wijers et al. (1997) take $F_{\nu,\rm max} \approx 5$ mJy based on the X-ray flux near the end of the initial γ-ray burst. The radio emission clearly did not reach this peak flux. Frail et al. (1998a) explain this result by claiming that $F_{\nu,\rm max}$ for the afterglow could not be estimated from the initial burst and that $F_{\nu,\rm max} \approx 20 - 40$ μJy. This requires a substantial gap in the X-ray evolution between the initial burst and the afterglow, and that the first optical observations have occurred shortly after ν_m passed through optical wavelengths. In a wind model, $F_{\nu,\rm max} \propto t^{-1/2}$ so there is a drop in $F_{\nu,\rm max}$ from the time of the early X-ray observations ($t \approx 50$ s) to the time of the radio observations. The radio limits can be accomodated even with an initially high X-ray flux in the afterglow.

4.2. GRB 970508

The optical afterglow of GRB 970508 followed power law evolution from day 2 to day $\gtrsim$100 with $\alpha = 1.141 \pm 0.014$ (Galama et al. 1998a). Galama et al. (1998b) compiled the radio to X-ray spectrum of the source on day 12.1 (see also Wijers & Galama 1999). The cooling frequency was at $\nu_c = 1.6 \times 10^{14}$ Hz or a wavelength of 2 μm, i.e. a frequency just below optical frequencies. Based on the day 12.1 spectrum, Galama et al. (1998b) estimate that $p = 2.2$, which yields $\alpha = -1.15$ and $\beta = -1.1$ for $\nu > \nu_c$ in both the $s = 0$ and $s = 2$ cases. The value of p is supported by both the observed spectrum and the rate of decline. However, because of the similar optical and X-ray evolution for ISM and wind interaction, radio observations are crucial for distinguishing between the $s = 0$ and $s = 2$ cases. Extensive radio data exist for GRB 970508, at 8.46, 4.86, and 1.43 GHz frequencies (Frail et al. 1997; Galama et al. 1998c; Waxman, Kulkarni, & Frail 1998; Kulkarni 1999). Here, we fit these radio data using the thin shell model of Li & Chevalier (1999) to determine the burst parameters. Our model treats synchrotron emission from a (trans-)relativistic blastwave propagating in an r^{-2} medium. Synchrotron self-absorption and relativistic effects are included, but not cooling. As usual, we take a power-law distribution of electron energy, and adopt an energy index of $p = 2.2$.

Since the observed radio frequencies are all below the cooling frequency ν_c in the time interval of interest, fitting the radio data alone fixes only three out of four parameters, as discussed in Li & Chevalier (1999). The additional constraint comes from the observed flux in the R-band, which is affected by cooling. Together, we find the best model parameters to be: $\epsilon_e = 0.37$, $\epsilon_{_B} = 0.01$, $E_{52} = 0.5$, and $A_\star = 0.8$ (which is in the expected range of a Wolf-Rayet star). The model fit is displayed in Fig. 1. The radio data before about day 100 are probably affected by strong scintillation. After about day 100, the fluxes at the two highest frequencies decline approximately as power-laws, and are fitted remarkably well by our model. The power-law index is close to -1.4, as expected for $p = 2.2$ in a constant-speed wind, but not in a constant density medium (where $t^{-0.9}$ is expected while the blast wave is relativistic). Approximately, the observed late time flux decline at 8.46 GHz follows

$$F_{8.46\ \mathrm{GHz}} \approx 500 \left(\frac{t}{100\ \mathrm{days}}\right)^{-1.4} \quad \mu\mathrm{Jy}, \tag{60}$$

which implies a flux in the R-band (with $\nu_{_R} = 4.5 \times 10^{14}$Hz) of

$$F_{_R} = \left(\frac{8.46 \times 10^9}{4.5 \times 10^{14}}\right)^{0.6} F_{8.46\ \mathrm{GHz}} \approx 0.73 \left(\frac{t}{100\ \mathrm{days}}\right)^{-1.4} \quad \mu\mathrm{Jy}, \tag{61}$$

if the R-band frequency is below the cooling frequency ν_c. The cooling frequency is estimated in equation (9) which, for the inferred parameters, becomes

$$\nu_c \approx 1.4 \times 10^{13} t_{\mathrm{day}}^{1/2} \ \ \mathrm{Hz}. \tag{62}$$

Setting $\nu_c = \nu_{_R}$, we obtain a cooling time $t_{_R} = 1000$ days for the R-band emission. After $t_{_R}$, $\nu_{_R} > \nu_c$, and the R-band flux is given by eq. (61). Before $t_{_R}$, we have $\nu_{_R} < \nu_c$, and the R-band flux is given instead by

$$F_{_R} = 0.73 \left(\frac{t_{_R}}{100\ \mathrm{days}}\right)^{-1.4} \left(\frac{t}{t_{_R}}\right)^{-1.15} = 82 t_{\mathrm{day}}^{-1.15} \ \ \mu\mathrm{Jy}. \tag{63}$$

This expected flux is shown in panel d of Fig. 1. Our model fits are reasonable overall in all four frequencies, lending support to the wind interaction scenario for this GRB. X-ray observations are expected to be compatible with our model because it is the same as an ISM model for $\nu > \nu_c$. The evolution between 6 hr and 6 days can be approximately fitted by $F_\nu \propto t^{-1.1\pm0.1}$ (Piro et al. 1998) and the optical/X-ray spectral index is compatible with $\beta_{oX} = -p/2 = -1.1$ (Galama et al. 1998b).

Galama et al. (1998b) end their paper advocating an $s = 0$ blast wave model for GRB 970508 by describing three deficiencies of the model: (1) $F_{\nu,\mathrm{max}}$ should be constant but is observed to decrease with time; (2) ν_A is predicted to be time-independent, but is observed to decrease with time, and the rise of the radio fluxes is slower than expected; and (3) the decay after maximum at mm wavelengths is perhaps somewhat faster than expected. All of these problems are addressed by the wind model, which provides approximate quantitative agreement with the observations.

Waxman et al. (1998) investigated a transition to nonrelativistic expansion as a possible reason for the deviations from the standard model, but found that this elaboration of the model did not explain the observations in a straightforward way.

Although the radio data appear to provide strong support for the wind model, the wind interpretation does give rise to possible problems regarding synchrotron cooling. In the wind model, ν_c increases with time; at optical wavelengths, a transition is expected from cooling evolution to adiabatic evolution. The opposite is true in $s = 0$ models. Galama et al. (1998b) cite evidence that ν_c evolves as expected in an $s = 0$ model. They identify an observed optical spectral transition between 1.0 and 1.8 days from $\beta = -0.54 \pm 0.14$ to $\beta = -1.12 \pm 0.04$ with the break frequency ν_c passing through the R_C band. The wind model would predict cooling in the R_C band at this early time and no transition. However, in the time before day 1.5, the observed light curve deviates strongly from standard afterglow models (e.g., Fruchter et al. 1999b and references therein) so that the early spectral index cannot be used as a constraint on models for the later power law evolution. Galama et al. (1998b) also cite moderately flat spectra between the K band (Chary et al. 1998) and R_C band on days 4.3 and 7.3 as supporting adiabatic evolution in the infrared at that time. This is in conflict with the wind model, but we believe that the overall weight of evidence supports the wind model. In the wind model, the optical spectrum should flatten and the light curve should steepen at late times.

Our model fails to account for the optical evolution before day 2 (e.g., Galama et al. 1998a; Fruchter et al. 1999b). At early times, the blast wave is expected to be in the fast cooling regime ($\nu_m > \nu_c$); this occurs at 500 s in the $s = 0$ model (Galama et al. 1998b), but at ~ 1 day in the wind model. Although the sharp rise in the light curve may be related to this transition, it is not possible to account for the rise in a straightforward way. In addition, Piro et al. (1999) have found possible evidence for redshifted iron line emission in the X-ray afterglow at an age ~ 1 day. In our model, the preshock density at that age is $\sim 7 \times 10^{-24}$ g cm^{-3}, which is orders of magnitude smaller than the density required for the line feature (Piro et al. 1999). As noted by Piro et al. (1999), ordinary stellar mass loss cannot account for the feature that they tentatively observe.

One expectation of the wind interaction model is that the event be accompanied by a supernova. However, Fruchter (1999) has found that a supernova like SN 1998bw added to the power law decline of the nonthermal afterglow emission would give an observable bump in the light curve at $t \sim 20 - 50$ days. Such a bump is not seen (Fruchter et al. 1999b) and a supernova in GRB 970508 would have to be about 1 magnitude fainter than SN 1998bw (Fruchter 1999). Considering possible differences in ejected mass, ^{56}Ni mass, and explosion energy, we believe that some variation in supernova properties is plausible.

A remarkable property of our model is that it approximately reproduces the light curve out to $t \approx 400$ days; there are a number of reasons why deviations from the model might be expected. First, if the ejecta initially cover a small solid angle, steepening of the light curve is expected as the blast wave slows (§ 2.5). Eq. (25) shows that $\theta \gtrsim 1$ is required to avoid the steepening; that is,

the blast wave is spherical or nearly so. Rhoads (1999) and Sari et al. (1999) reached a similar conclusion for GRB 970508 based on an interstellar interaction model for the source. If the slowing proceeds to nonrelativistic expansion, a steepening of the light curve is again expected (§ 2.4). From eq. (23), the transition to nonrelativistic expansion occurs at $t_{NR} \approx 2.8$ yr. A relativistic model is thus expected to apply throughout the period of observation. Finally, the blast wave must remain within the steady stellar wind. From eq. (4) and the blast wave parameters, the observed shock has $R \approx 5 \times 10^{18}$ cm. The discussion in CL shows that the wind can plausibly extend to this distance.

4.3. GRB 990123

The afterglow of GRB 990123 was briefly discussed by CL as a probable case of ISM interaction. The observations over the time period $0.01 - 1.5$ day (Kulkarni et al. 1999; Galama et al. 1999a; Castro-Tirado et al. 1999) can be fitted by an ISM interaction model with $p = 2.5$ and optical wavelengths in the adiabatic regime ($\alpha = -1.12$; $\beta = -0.75$) and X-ray wavelengths in the cooling regime ($\alpha = -1.38$; $\beta = -1.25$). The observed steeper decline in the X-rays vs. the R band ($\alpha = -1.44 \pm 0.07$ vs. $\alpha = -1.10 \pm 0.03$, Kulkarni et al. 1999) is expected for ISM interaction, but not for wind interaction.

A new feature observed in GRB 990123 was a 9th magnitude optical flash overlapping with the GRB (Akerlof et al. 1999). Sari & Piran (1999) and Mészáros & Rees (1999) found that the properties of the optical emission over the first ~ 15 minutes could be modeled by synchrotron emission from the reverse shock front resulting from interaction with a constant density, interstellar medium. In § 3 here, we find it difficult to produce such a strong synchrotron, optical flash with standard parameters. If we let $z = 1.6$, $X = 0$, $\phi_p = 0.6$ and $\Delta_{10} = 4$ (so that the emission peaks around 50 s, as observed), and assume $A_\star = \gamma_{300} = 1$ and $\epsilon_B = 0.1$, then an explosion energy of 10^{54} ergs is required to produce the 9th magnitude optical flash. Such an energy is two orders of magnitude higher than the standard value, but it may not be a problem for GRB 990123, the brightest γ-ray burst with well localized position. The estimated γ-ray energy alone for this source ranges from $\sim 10^{53}$ (with beaming) to $\sim 3 \times 10^{54}$ ergs (isotropic; Kulkarni et al. 1999). The explosion energy could be substantially higher. Therefore, the magnitude of the optical flash does not provide a clear discriminator between wind interaction and interstellar interaction in this case.

The observed temporal behavior of the optical flash of GRB 990123 is not compatible with the predictions of wind interaction model. The flash is predicted to rise with time as $t^{1/2}$ (assuming that self-absorption is not significant, which is approximately true for the parameters listed in the preceding paragraph), whereas the observed rise is much steeper, close to $t^{3.7}$. In addition, the emission from the reverse shock is short-lived in a wind interaction model and is not compatible with the observed t^{-2} flux evolution over the first 15 minutes (Akerlof et al. 1999, Sari & Piran 1999a; § 3).

4.4. GRB 990510

The optical afterglow of GRB 990510 was well-observed in the first 4 days after the burst (Stanek et al. 1999; Harrison et al. 1999). The light curve could be well-fitted by an initial power law $F_\nu \propto t^{\alpha_1}$ followed by a steepening to another power law $F_\nu \propto t^{\alpha_2}$. Although there was considerable overlap in the data that they used for their analyses, Stanek et al. (1999) found $\alpha_1 = -0.76 \pm 0.01$ and $\alpha_2 = -2.40 \pm 0.02$ while Harrison et al. (1999) found $\alpha_1 = -0.82 \pm 0.02$ and $\alpha_2 = -2.18 \pm 0.05$. The initial flat evolution is strongly suggestive of adiabatic evolution ($\nu_m < \nu < \nu_c$) in a constant density medium ($F_\nu \propto t^{-3(p-1)/4}$). The initial decline rate measured by Harrison et al. (1999) is then consistent with $p = 2.1$ and with the later evolution being due to a slowed jet with $F_\nu \propto t^{-p}$ (Sari et al. 1999). The results of Stanek et al. (1999) suggest a somewhat smaller value of p from the early evolution and a somewhat larger value of p from the later evolution, but they are close to the expected evolution. The value $p = 2.1$ implies $F_\nu \propto \nu^{-0.55}$, which is consistent with the spectrum $F_\nu \propto \nu^{-0.61\pm0.12}$ measured from BVRI photometry (Stanek et al. 1999). The hypothesis of jet evolution is supported by radio data which are consistent with the expected $F_\nu \propto t^{-1/3}$ evolution (Harrison et al. 1999).

Evolution in a constant density medium thus gives a consistent picture for this afterglow. Evolution in a wind cannot plausibly account for the early flat decline, even taking into account the possibility of being in the strong cooling regime (§ 2.2 and 2.3).

The steepening of the afterglow light curve to $\alpha_2 = -2.2$ after 1.4 days should have facilitated the observation of a supernova above the nonthermal emission. Our model would predict the absence of such a supernova if it was an interstellar interactor, but a test is difficult because of the high redshift of the event, $z = 1.619$ (Vreeswijk et al. 1999). *HST* observations by Fruchter et al. (1999c) showed that on 17.9 June, 1999 (day 38.5) the afterglow flux was somewhat above the extrapolation of the t^{α_2} decline, but the excess counts were a factor 7 below what would be expected if a supernova like SN 1998bw were present.

4.5. Discussion

A summary of the results from this section is in Table 1. In addition to the sources discussed here, we have added GRB 980425 (Kulkarni et al. 1998; Li & Chevalier 1999) and GRBs 980326 and 980519 (CL). The redshift is given in column 2 for those for which it has been determined (see the recent compilation of Ghisellini 1999 for references). The next column gives the afterglow type, as determined by the afterglow evolution. We claim that GRBs 970228 and 970508 are probable wind interactors, although they have been widely interpreted in terms of interstellar interaction in the literature. The reasons for this are varied. In the case of GRB 970228, the recognition of supernova emission in the optical light curve yields a steeper nonthermal afterglow decline, in line with expectations for wind interaction. In the case of GRB 970508, the cooling frequency ν_c is somewhat below optical wavelengths so that the high frequency evolution is the same for wind

and interstellar interaction. However, the predicted evolution is different at radio wavelengths and the radio data clearly indicate wind interaction. The radio data are crucial for typing this burst, as they are for the afterglow of GRB 980519. We have examined the data available on other sources, but have not found more that can be reliably typed. The afterglow of GRB 971214 was extensively observed at optical wavelengths, but there is probably significant extinction in the host galaxy and radio data are not available. The afterglow of GRB 980329 was observed at radio wavelengths; the 8.3 and 4.9 GHz data of Taylor et al. (1998) over the first 30 days appear to be in the self-absorbed regime. The data appear to be better approximated by $F_\nu \propto t^{1/2}$ evolution (interstellar) as opposed to $F_\nu \propto t$, but there are strong scintillation effects. The higher frequency data are difficult to model. Dai & Lu (1998) suggested that GRB 970616 is a wind interactor based on the steep decline with time indicated by two X-ray flux measurements; we believe that more detailed observations are needed to make an identification.

Column 4 of Table 1 shows that the estimated electron energy spectral index, p, varies over the set of bursts. The probable error in these estimates, ~ 0.1, cannot account for the range. The high values of p for GRBs 980326 and 980519 are reduced in jet models for these sources (Sari et al. 1999), but a range in p of at least $\sim 2.1 - 2.5$ is difficult to avoid. The lack of a universal value for p calls into question the initial assumption that the shock front accelerates electrons to a power law above γ_m that is constant with energy and with time. The possibility of curvature in the spectrum and/or time evolution of p should be examined as the data on GRB afterglows improve.

Column 5 indicates whether there is evidence for a supernova like SN 1998bw in the emission from the source. The case is clearest for GRB 980425 and its probable association with SN 1998bw. The data on GRB 970228 are compatible with a supernova very much like SN 1998bw (Reichart 1999; Galama et al. 1999b). This is also true for GRB 980326, although the observational case is not as clear (Bloom et al. 1999b). CL noted that the last reported optical observation of GRB 980519 may be due to a supernova, but this hypothesis has not yet been checked. The fact that GRB 970508 does not show evidence for a supernova like SN 1998bw appears to contradict the expectations of our model. However, the nonthermal optical emission was strong, so that a supernova somewhat fainter than SN 1998bw can be accomodated. Supernovae associated with GRBs can be expected to have a range of properties; some variation in explosion energy, ejected mass, and mass of ^{56}Ni are all plausible.

The sixth column lists whether a prompt, optical flash was observed. Such an event has been seen only in GRB 990123 and was attributed to synchrotron emission from the reverse shock wave (Sari & Piran 1999a; Mészáros & Rees 1999). In our picture, the bursts with a wind type afterglow would have a weaker optical synchrotron emission from the reverse shock wave than the bursts with an interstellar type afterglow of similar burst parameters. Unfortunately, there do not appear to be any existing observations to test this hypothesis and future observations are needed to provide a test.

The last column of Table 1 lists whether there is evidence for a jet in the afterglow evolution.

The entry "No" indicates that the jet opening angle is $\theta_o \gtrsim 1$. The case of GRB 970508 was discussed by Rhoads (1999) and Sari et al. (1999) for ISM interaction and in § 4.2 for wind interaction. Li & Chevalier (1999) found that semi-relativistic, spherically symmetric models provided a good description of SN 1998bw/GRB 980425. GRBs 990123 and 990510 show probable jet effects on a timescale $\sim 1-2$ days (Kulkarni et al. 1999; Harrison et al. 1999; Sari et al. 1999). The cases of GRBs 980326 and 980519 are controversial. If the steep declines of their optical afterglows are interpreted as jet effects (Sari et al. 1999) then the jet effects occur at an earlier time than for GRBs 990123 and 990510, but if the declines are interpreted as wind interaction (CL and this paper) then the jet effects occur later if at all.

5. TWO TYPES OF PROGENITORS

In CL, we suggested that there are two types of GRB progenitors among the well-observed sources: massive stars that have afterglows characteristic of wind interaction and are likely to be accompanied by supernovae, and compact binary mergers that have afterglows characteristic of constant density, interstellar interaction and are not accompanied by supernovae. Our discussion here has increased the wind group by adding GRBs 970228 and 970508. The pattern of association with a supernova is strengthened by the finding of strong evidence for a supernova in GRB 970228. A new result here is that the prompt optical flash in a wind interaction GRB is expected to rise slowly and to disappear adruptly, in contrast to the observed temporal behavior of the optical flash of GRB 990123. The contradiction points to an interstellar interaction for this case, which supports the interpretation of the afterglow light curve evolution by CL.

Another possible indicator of the GRB progenitor type is the location in a galaxy (Paczyński 1998). For the cases in which imaging with *HST* is available, the bursts appear to be superposed on or near the optical disks of the host galaxies. In the case of GRB 990123, the burst is at about 5.8 kpc ($0.''67$) from the center of the host galaxy, near the edge of the optical disk (Bloom et al. 1999a). In the case of GRB 990510, no host galaxy has been detected, even with deep imaging (Israel et al. 1999; Fruchter et al. 1999c). However, the production of a typical afterglow for the interstellar interaction case probably requires that the burst take place in or near a galaxy so that the surrounding density is sufficiently high. For GRB 970508, which we have identified as a wind interactor, the burst is within $0.''01$, or 70 pc of the galaxy center (Fruchter et al. 1999b). Wind interaction implies a massive star progenitor and the source may have been in a nuclear starburst region. In the case of GRB 970228, the source is about $0.''5$ from the galaxy center (Sahu et al. 1997), which is comparable to the interstellar interaction case of GRB 990123. Location does not appear to provide a clear discriminator for the two types of bursts considered here.

We have argued that there are two types of burst progenitors, so the GRBs associated with the two types might be expected to have distinct properties. We have examined the data on the GRBs themselves and have found no clear distinction between those that give rise to wind or to ISM type afterglows. In both cases, the γ-ray light curves are complex and last for 10's of seconds.

One implication is that the mechanism giving rise to the initial GRBs does not depend on the external medium. This supports the generally favored internal shock model for the GRBs (e.g., Piran 1999).

Another implication is that, for both types, the source must be capable of producing a long duration burst. This is expected for a massive star origin because the collapse time of the stellar core is on the order of 10's of seconds (MacFadyen & Woosley 1999; Fryer, Woosley, & Hartmann 1999a). Among the compact binary mergers that have been proposed (Fryer et al. 1999a and references therein), the type that may satisfy the duration requirement is the black hole - white dwarf merger (Fryer et al. 1999b). In addition, this type of merger is expected to occur in or near the host galaxy, again in accord with observations. For the small number of sources we have discussed here, the rate of massive star explosions is not very different from the rate of compact star explosions. However, the interstellar interactors are somewhat more distant and luminous than the wind interactors on average, and the occurrence of GRB 980425/SN 1998bw indicates the presence of low energy wind interactors. This would imply a higher rate of massive star explosions per unit volume than of compact star explosions. However, if jet effects are more important for interstellar interactors (as suggested by Table 1), the rate of interstellar interactors is increased, so no clear conclusions are possible for the relative rates.

One of the unexpected results of this study is the possible evidence for for a relation between jet effects and the afterglow (and thus progenitor) type. Based on a small number of objects, the interstellar interactors show evidence for significant jet effects, while the wind interactors with massive star progenitors do not. This suggests the intriguing possibility that the GRB engine generates a collimated flow, but in the case of a massive star progenitor the flow becomes uncollimated upon passing through the star.

6. CONCLUSIONS

The results of our work can be summarized as follows:

1. The afterglow light curves resulting from the interaction of a GRB with a circumstellar wind have properties that depend on the observation frequency. At radio frequencies, there are two possibilities. Above ν_{Am} (eq. [17]), the light curve has 3 segments: $F_\nu \propto \nu^2 t$ ($t < t_A$), $F_\nu \propto \nu^{1/3} t^0$ ($t_A < t < t_m$), $F_\nu \propto \nu^{-(p-1)/2} t^{-(3p-1)/4}$ ($t_m < t$), where p is the electron spectral index. Detailed integrations over a spherical blast wave show these segments, but without sharp transitions. Below ν_{Am}, the middle, flat evolution phase is not present. At high frequencies (optical and X-ray), the evolution may make a transition from cooling ($F_\nu \propto \nu^{-p/2} t^{-(3p-2)/4}$) to adiabatic ($F_\nu \propto \nu^{-(p-1)/2} t^{-(3p-1)/4}$) evolution, or may remain in one of these phases depending on the parameters, especially ϵ_B. The transition occurs earlier at lower frequency. For typical parameters, the fast cooling phase (all electrons cool) lasts for ~ 1 day, considerably longer than in the interstellar interaction case. The light curve can be modified from the above expressions

during this early phase.

2. During wind interaction, the transition to nonrelativistic evolution occurs at ~ 2 yr for typical parameters. This is longer than in the interstellar interaction case because of the low density in the outer parts of the wind.

3. The optical synchrotron emission from the early reverse shock wave is weaker for wind interaction than for interstellar interaction, giving a source with optical magnitude ~ 13.5 or fainter for standard parameters. Radio emission is strongly self-absorbed during this phase.

4. The recognition of supernova emission in the optical radiation from GRB 970228 (Reichart 1999; Galama et al. 1999b) implies that the decline of the nonthermal afterglow is faster than previously thought and is compatible with adiabatic wind interaction.

5. The optical spectrum and decline over days $2 - 100$ of GRB 970508 suggest cooling evolution and are compatible with either interstellar or wind interaction models. However, the extensive radio data on this source strongly suggest wind interaction. In our model, the blast wave energy is 5×10^{51} ergs and the wind mass loss rate is 8×10^{-6} $M_\odot$ yr^{-1} for a wind velocity of $1,000$ km s^{-1}.

6. In the case of GRB 990123, the afterglow showed a steeper decline with time in X-rays than in optical emission, as expected for interaction with a constant density medium. A prompt optical flash was observed from this object, which can be plausibly attributed to synchrotron emission from the reverse shock front due to interaction with the interstellar medium (Sari & Piran 1999a,b). We have found that interaction with a wind cannot produce the temporal behavior of the observed flash. The case for interstellar interaction appears to be strong. We have also identified GRB 990510 as a likely interstellar interactor based on its early time evolution.

7. Among the 7 sources for which we have suggested identifications, 5 are wind interactors and 2 are interstellar interactors. The interstellar interactors are somewhat more luminous and distant, but appear to have more significant jet effects, so no clear conclusions can be drawn regarding the relative rates of the two types. However, there does not appear to be a clear distinction in the initial γ-ray burst properties of these different types. This provides additional evidence for a burst model that does not depend on environment, e.g., the internal shock model for bursts.

The main result of our paper is the presentation of evidence for two types of GRB afterglows in different environments: a constant density interstellar medium and the wind of a Wolf-Rayet star. The types are not immediately distinguishable because at an age of a few days, the preshock wind density is comparable to an interstellar density. At an age of seconds, the preshock density is higher for the wind case and we predict that the wind interactors have fainter prompt optical emission than the interstellar interactors with similar burst parameters. In addition, we expect the wind interactors to be accompanied by a supernova event. Future observations of GRBs and their afterglows should provide a clear test of our model.

We are grateful to Dale Frail and Andy Fruchter for useful correspondence. Support for this work was provided in part by NASA grant NAG5-8232.

Table 1. Properties of GRB Afterglows

Burst GRB	Redshift z	Afterglow Type	Spectral Index, p	Supernova like SN 1998bw	Prompt, Bright Optical Flash	Jet
970228	0.695	Wind	2.6	Yes		
970508	0.835	Wind	2.2	No		No
980326		Wind	3.0	Yes		
980425	0.0085	Wind	2.5	Yes		No
980519		Wind	3.0	?		
990123	1.60	ISM	2.5		Yes	Yes
990510	1.619	ISM	2.1	No		Yes

REFERENCES

Akerlof, C. W., et al. 1999, Nature, 398, 400

Blandford, R. D., & McKee, C. F. 1976, Phys. Fluids, 19, 1130

Bloom, J. S., et al. 1999a, ApJ, 518, L1

Bloom, J. S., et al. 1999b, Nature, in press

Castro-Tirado, A. J., et al. 1999, Science, 283, 2069

Chary, R., et al. 1998, ApJ, 498, L9

Chevalier, R. A., & Li, Z.-Y. 1999, ApJ, 520, L29 (CL)

Costa, E., et al. 1997, Nature, 387, 783

Dai, Z. G., & Lu, T. 1998, MNRAS, 298, 87

Frail, D. A., Kulkarni, S. R., Nicastro, L., Feroci, M., & Taylor, G. B. 1997, Nature, 389, 261

Frail, D. A., Kulkarni, S. R., Shepherd, D. S., & Waxman, E. 1998a, ApJ, 502, L119

Frail, D. A., Taylor, G. B., Kulkarni, S. R., et al. 1998b, GCN Circ. 89

Frontera, F., et al. 1998, A&A, 334, L69

Fruchter, A. S. 1999, talk at STScI Symposium on The Largest Explosions Since the Big Bang: Supernovae and Gamma-Ray Bursts

Fruchter, A. S., et al. 1999a, ApJ, 516, 683

Fruchter, A. S., et al. 1999b, preprint (astro-ph/9903236)

Fruchter, A. S., Ferguson, H., Pepper, J., Gibbons, R., Sahu, K., Pian, E., et al. 1999c, GCN Circ. 386

Fryer, C. L., Woosley, S. E., & Hartmann, D. H. 1999a, ApJ, in press (astro-ph/9904122)

Fryer, C. L., Woosley, S. E., Herant, M., & Davies, M. B. 1999b, ApJ, 520, 650

Galama, T. J., et al. 1998a, ApJ, 497, L13

Galama, T. J., Wijers, R. A. M. J., Bremer, M., Groot, P. J., Strom, R. G., Kouveliotou, C., & van Paradijs, J. 1998b, ApJ, 500, L97

Galama, T. J., et al. 1998c, ApJ, 500, L101

Galama, T. J., et al. 1998d, Nature, 395,670

Galama, T. J., et al. 1999a, Nature, 398, 394

Galama, T. J., et al. 1999b, ApJ, submitted (astro-ph/9907264)

Ghisellini, G. 1999, preprint (astro-ph/9907376)

Granot, J., Piran, T., & Sari, R. 1999, ApJ, submitted (astro-ph/9808007)

Halpern, J. P., Kemp, J., Piran, T., & Bershady, M. A. 1999, ApJ, 517, L105

Harrison, F. A., et al. 1999, ApJ, in press (astro-ph/9905306)

Israel, G. L., et al. 1999, A&A, submitted (astro-ph/9906409)

Katz, J. I. 1994, ApJ, 422, 248

Kulkarni, S. R. 1999, talk at ITP Conf. on Gamma-Ray Bursts and their Afterglows (http://www.itp.ucsb.edu/online/gamma_c99/kulkarni/)

Kulkarni, S. R., Frail, D. A., Wieringa, M. H., Ekers, R. D., Sadler, E. M., Wark, R. M., Higdon, J. L., Phinney, E. S., & Bloom, J. S. 1998, Nature, 395, 663

Kulkarni, S. R., et al. 1999, Nature, 398, 389

Li, Z.-Y., & Chevalier, R. A. 1999, ApJ, in press (astro-ph/9903483)

MacFadyen, A., & Woosley, S. E. 1999, ApJ, in press (astro-ph/9810274)

Mészáros, P. & Rees, M. J. 1997, ApJ, 476, 232

Mészáros, P. & Rees, M. J. 1999, MNRAS, 306, L39

Mészáros, P., Rees, M. J., & Wijers, R. A. M. J. 1998, ApJ, 499, 301

Paczyński, B. 1998, ApJ, 494, L45

Panaitescu, A., Mészáros, P., & Rees, M. J. 1998, ApJ, 503, 315

Panaitescu, A., & Mészáros, P. 1999, ApJ, 526, in press (astro-ph/9806016)

Piran, T. 1999, Phys. Rep., 314, 575

Piro, L., et al. 1998, A&A, 331, L41

Piro, L., et al. 1999, ApJ, 514, L73

Reichart, D. E. 1999, ApJ, 521, L111

Rhoads, J. E. 1997, ApJ, 487, L1

Rhoads, J. E. 1999, ApJ, in press (astro-ph/9903399)

Sahu, K. C., et al. 1997, Nature, 387, 476

Sari, R. 1997, ApJ, 489, L37

Sari, R. 1998, ApJ, 494, L49

Sari, R. & Piran, T. 1995, ApJ, 455, L143

Sari, R. & Piran, T. 1999a, ApJ, 517, L109

Sari, R. & Piran, T. 1999b, ApJ, 520, 641

Sari, R., Piran, T., & Halpern, J. P. 1999, ApJ, 519, L17

Sari, R., Piran, T., & Narayan, R. 1998, ApJ, 497, L17

Sedov, L. I. 1959, Similarity and Dimensional Methods in Mechanics (New York: Academic)

Sokolov, V. V., Kopylov, A. I., Zharikov, S. V., Feroci, M., Nicastro, L., & Palazzi, E. 1998, AA, 334, 117

Stanek, K. Z., Garnavich, P. M., Kaluzny, J., Pych, W., & Thompson, I. 1999, ApJ, 522, L39

Taylor, G. B., Frail, D. A., Kulkarni, S. R., Shepherd, D. S., Feroci, M., & Frontera, F. 1998, ApJ, 502, L115

Vietri, M. 1997, 488, L105

Vreeswijk, P., et al. 1999, GCN Circ. 324

Waxman, E. 1997, ApJ, 489, L33

Waxman, E., Kulkarni, S. R., & Frail, D. A. 1998, ApJ, 497, 288

Wijers, R. A. M. J., & Galama, T. J. 1999, ApJ, submitted (astro-ph/9805341)

Wijers, R. A. M. J., Rees, M. J., & Mészáros, P. 1997, MNRAS, 288, L51

Woosley, S. E. 1993, ApJ, 405, 273

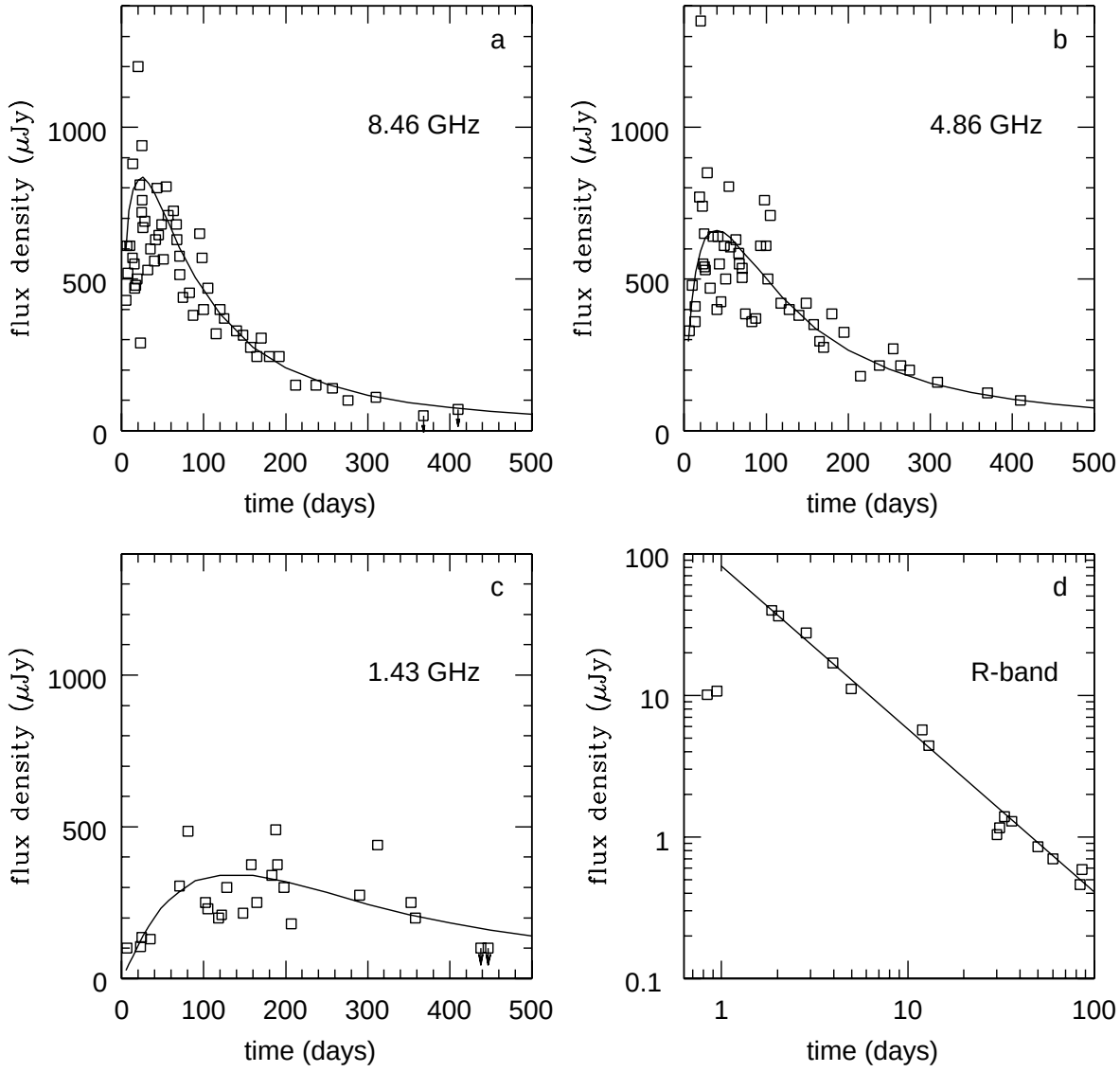

Fig. 1.— Wind interaction model for the afterglow of GRB 970508. Radio data before about day 90 are taken from Frail et al. (1997); the rest are estimated from a viewgraph presented by Kulkarni (1999). R-band data are taken from Sokolov et al. (1998). The best model fit parameters are listed in the text.